*Preprints Volume, 16th Conf. on Severe Local Storms & the Conf. on Atmospheric Electricity,* Kananaskis Park, CANADA, AMS Oct. 22-26, 1990, 467-472.

12.1

# SEVERE LEFT-MOVING HAILSTORMS IN CENTRAL SWITZERLAND

**W. Schmid and H.-H. Schiesser**

Atmospheric Physics, Swiss Federal College of Technology
CH-8093 Zurich, Switzerland

**R.A. Houze, Jr. and R.G. Fovell**

Atmospheric Sciences, University of Washington
Seattle, WA 98195, USA.

## 1. INTRODUCTION

Severe thunderstorms in the midlatitudes tend to travel to the right or to the left with respect to the direction of the mean environmental winds (Browning 1968). The Northern-hemispheric severe right-moving storms (SR storms) have been investigated by many authors, whereas the literature about their left-moving counterparts (e.g. Achtemeier 1975; Tripoli and Cotton 1986) is much less extensive. One could conclude that the SR storms are more frequent than the severe left-moving storms (SL storms) in the Northern hemisphere. While this may be correct for tornadic storms in the central U.S. (e.g. Maddox 1976), there exists a considerable lack of knowledge about the relative frequency of left- and right-moving storms in the case of severe hailstorms. No reference could be found which indicates the number of right- and left-moving hailstorms within a given area and the climatologically significant time interval. This lack of information may be because of the sporadic occurrence of severe hailstorms and the difficulty identifying radar-observed storms as severe hailstorms. Several years of radar data and ground-truth data are needed in order to obtain a representative data sample.

The main purpose of the present paper is to document the motion of severe hailstorms that occurred in central Switzerland during 1975-1982. It will be shown that the frequency and severity of SL storms is almost as large as the frequency and severity of the SR storms. In order to understand this surprising result, the characteristics of the storms are described and related to the mean hodographs of the representative soundings. A numerical model is employed to aid in these interpretations.

## 2. IDENTIFICATION OF SL AND SR HAILSTORMS

A carefully calibrated S-band weather radar was operated during the preparatory and active phases of the hail suppression experiment *Grossversuch* IV (Federer et al. 1986). The radar was designed to measure parameters of hailfall intensity with a high spatial and temporal resolution. The mode of operation of the radar was adapted to this purpose, and only minor procedural changes were made during the eight-year period. Frequent PPI scans at low elevation angles were preferred to less-frequent volume scans. The range of the radar measurements was restricted to 60 km. Major efforts were undertaken to calibrate the radar and to investigate the relationship between hailpad and radar measurements of hailfall parameters. Long-term raindrop distrometer data were used to assess the temporal stability of the radar. An overall uncertainty of the radar measurements on the order of $\pm$ 1 dBZ was obtained (Waldvogel and Schmid 1982). The agreement between radar and hailpad measurements of global-hail kinetic energy was found to be excellent (Waldvogel et al. 1978; Waldvogel and Schmid 1983). Generally, radar reflectivities larger than 60 dBZ indicated damaging hailfall at the ground (Schiesser 1990). This criterion is in excellent agreement with other studies of the relationship between radar and ground measurements of hail (e.g. Aydin et al. 1986).

Since the intensity of hailfall can be estimated with a high degree of accuracy from the measurements of radar reflectivity alone, a "severe hailstorm" is defined here only in terms of the characteristics of the radar measurements. This makes the search through the radar data sample both objective and simple. A "45 dBZ cell" (Waldvogel and Schmid 1982) is classified as a severe hailstorm when its maximum reflectivity exceeds 65 dBZ and when the 60 dBZ intensity is sustained for at least 30 min. The second criterion eliminates single-cell storms (Chisholm and Renick 1972) and ensures that the storm reaches some degree of self-regeneration. Available hail ground-truth data (hailpad networks, insurance data of hail damage, and public reports) confirm that this definition is appropriate and selects the most damaging hailfalls observed during the period of *Grossversuch* IV.

The classification of severe thunderstorms as SL or SR storms can be made following the scheme given by Browning (1968). A careful inspection of the radar pattern and of the representative wind hodograph is required. We found that the radar observations were sufficient to classify the storms in many cases. The radar patterns of these severe thunderstorms are normally highly asymmetrical. The reflectivity core and the high-reflectivity gradients are near the upwind edge of the storms, while the downwind flank of the storm is characterized by a low-gradient reflectivity pattern, apparently consisting of precipitation from the anvil. This typical echo pattern is used to estimate the environmental mean-wind vector (EW) for each storm. A vector is fixed, pointing from the reflectivity core of a storm towards the downwind center of the anvil echo. This vector is an indicator of the direction of the mean storm-relative environmental winds and is assumed to be the EW. Each storm is then classified as SL or SR rather simply by comparing the vector of the storm movement with the EW vector (see the examples given in Fig. 1).

This scheme has been applied to the available "severe hailstorm" data from *Grossversuch* IV. Only those storms whose radar-echo structures were simple enough to determine EW by the above method during the time that their maximum intensity exceeded 60 dBZ have been considered. In nearly all cases for which it was feasible to compare the radar-estimated EW to rawinsonde data, the decision made with the radar data alone agreed with the observed wind hodographs. In one case, (the cell 1346 from June 10, 1979, in Table 1), the vector of the storm movement coincided with the radar-defined EW vector, but the classification could be made by considering the representative wind hodograph.

## 3. PROPERTIES OF SL AND SR HAILSTORMS

### *3.1 Radar structure*

This section summarizes some characteristic radar features of the "Swiss type" severe hailstorms. The radar data in Fig. 1 illustrate these features reasonably well. Both scans were obtained shortly before the storms reached their maximum intensity. To a first approximation, the SL storm can be considered a mirror image of its right-moving counterpart, with respect to the movement of the storms and the location of their general structural features. One aspect, however, does not fit the "mirror image" hypothesis. The SL storm shows a distinct "hook" echo on the southwestern (right-rear) flank. The radar pattern of this storm thus appears to resemble the radar pattern of a tornadic SR storm, which has a mesocyclone associated with a hook echo on its right flank (see the example in Fig. 1 in Lemon and Doswell 1979). The hook echo in the Swiss SL storm developed from small-scale radar-echo features rotating counterclockwise from the northwestern edge along the upwind border of the storm. One could conclude that the SL storm shown in Fig. 1 has a similar internal structure to the tornadic SR storm. This conclusion, however, would contradict the "mirror image" hypothesis. The example of Fig. 1 is not a singular case showing a hook-echo

Table 1: The SL and the SR hailstorms in central Switzerland (1975-1982). (1) refers to the time when the reflectivity level of the 60 dBZ was first observed. A (D) indicates that the storm produced hail damage at the ground which has been registered by the Swiss Hail Insurance Company. In column (2) an asterisk marks the storms which apparently entered or left the radar range. The resolution of the archived maximum reflectivity (Zm) was improved from 3-5 dBZ in 1975-1977 to 1 dBZ in 1978.

**SL Storms**

| Date M/DD/YY | Cell (1) | t > 59dBZ (min) (2) | Zm (dBZ) (3) | Movement (Deg/m s$^{-1}$) |
|---|---|---|---|---|
| 7/08/75 | 2035D | 51 | >70 | 211/12.2 |
| 7/09/75 | 2115D | 66 | >70 | 194/5.6 |
| 7/10/75 | 1450D | 76 | >65 | 225/5.2 |
| 7/15/75 | 1500D | 86 | >65 | 235/12.7 |
| 7/15/75 | 2015D | 91 | >65 | 225/13.1 |
| 8/01/75 | 1440D | 51 | >65 | 279/12.0 |
| 8/01/75 | 1600D | 61 | >65 | 276/12.6 |
| 8/06/77 | 1828D | 48 | >65 | 221/5.8 |
| 6/09/78 | 1904D | 44* | 68 | 246/15.9 |
| 7/14/78 | 1703 | 38 | 71 | 248/7.8 |
| 7/14/78 | 1743D | 153* | 71 | 249/7.8 |
| 7/14/78 | 1815 | 101* | 71 | 248/8.1 |
| 7/18/78 | 1128 | 47 | 66 | 247/20.0 |
| 7/18/78 | 1453 | 71* | 67 | 228/16.6 |
| 6/10/79 | 1346D | 70 | 69 | 225/7.6 |
| 6/26/79 | 1814D | 47* | 71 | 224/8.4 |
| 8/07/79 | 1904D | 61 | 69 | 210/4.9 |
| 8/07/79 | 1906D | 59 | 68 | 230/8.5 |
| 7/15/82 | 1509D | 115 | 73 | 198/7.5 |
| 7/16/82 | 1814D | 117* | 73 | 219/9.6 |

**SR Storms**

| Date M/DD/YY | Cell (1) | t > 59dBZ (min) (2) | Zm (dBZ) (3) | Movement (Deg/ms$^{-1}$) |
|---|---|---|---|---|
| 7/08/75 | 2015D | 51 | >65 | 276/7.2 |
| 7/09/75 | 1715D | 81* | >65 | 278/7.3 |
| 7/11/75 | 1350D | 66* | >65 | 300/5.4 |
| 7/15/75 | 1950D | 66 | >65 | 286/11.7 |
| 5/19/76 | 1445D | 104 | >70 | 228/6.5 |
| 8/16/77 | 1940D | 44* | >68 | 282/10.9 |
| 8/17/77 | 1650D | 44* | >68 | 236/12.9 |
| 6/09/78 | 2115 | 43 | 72 | 279/15.9 |
| 7/14/78 | 1554D | 136* | 73 | 290/11.3 |
| 7/18/78 | 1138D | 54* | 77 | 257/17.7 |
| 7/18/78 | 1215D | 52* | 73 | 259/19.8 |
| 7/18/78 | 1228D | 94* | 75 | 260/16.3 |
| 7/18/78 | 1453 | 64* | 73 | 257/15.7 |
| 8/06/78 | 1752D | 63* | 74 | 262/13.5 |
| 8/06/78 | 1819D | 74 | 73 | 255/16.1 |
| 8/07/79 | 1747 | 61* | 67 | 268/7.0 |
| 8/07/79 | 1818D | 106 | 69 | 279/8.6 |
| 9/09/79 | 1946D | 97 | 72 | 280/7.3 |
| 6/03/81 | 2008D | 116 | 69 | 221/10.4 |
| 8/08/81 | 1618D | 48* | 73 | 248/8.9 |
| 6/22/82 | 1648D | 51* | 68 | 237/15.2 |
| 7/16/82 | 2002D | 33 | 71 | 280/6.9 |

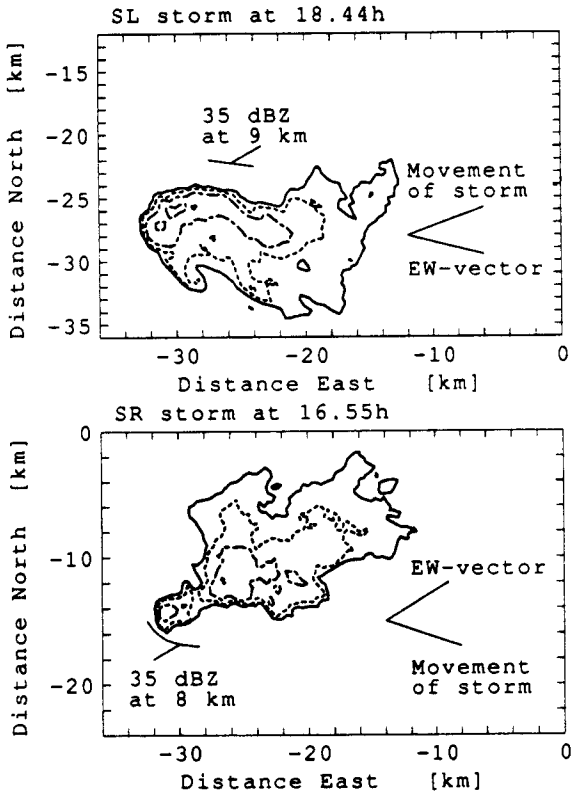


***Fig. 1**: The PPI radar contours 35, 45, 55, and 65 dBZ of two severe hailstorms which have been scanned on July 14, 1978 at an altitude of approximately 3 km msl (2 km above ground).*

structure. At present, the kinematical and dynamical structure of the "Swiss type" SL storm remains a mystery. Doppler-radar measurements within such storms are planned for the near future.

### *3.2 Statistical analysis*

In all, 42 severe hailstorms were identified in the eight years of data from *Grossversuch* IV. Of these, 20 were identified as SL storms by the above techniques. Thus, we find that nearly half of the severe hailstorms in central Switzerland are left-moving! Some characteristic parameters of the individually identified SL and SR storms are given in Table 1. Table 2 presents mean values and standard deviations of the maximum reflectivity; the time for which the storm exceeded 60 dBZ and the direction and speed of storm movement. The movement of the storms was determined from the storm locations at the time when the first and last appearance of the 60 dBZ level was observed. A Wilcoxon test was applied to the data in order to find significant differences in between the defined parameters. No significant differences could be detected with respect to the duration or speed of the two storm classes. The directions of storm movement, however, differ significantly—as expected. The values of the maximum reflectivity are somewhat higher for the SR storms than for the SL storms. However, the 5% level of significance is not reached. The difference is associated with the storms of 9 June 1978 and 18 July 1978. The SR storms on these two days were stronger than the corresponding SL storms. Further inspection of Table 1 indicates that the storms occurring on those two days moved at an unusually high speed (> 15 m s$^{-1}$). Excluding the data from 9 June 1978 and 18 July 1978 yields a difference of only 0.5 dBZ between the mean values of the maximum reflectivity. Thus, no significant differences can be found with respect to the maximum reflectivity as long as the storm movement is < 15 m s$^{-1}$. Since the faster-moving storms are an exception within the data sample of Table 1, the apparent difference in the maximum reflectivity of these storms must be accepted with caution.

## 4. MEAN HODOGRAPHS

Vector averages of rotated hodographs of the most representative soundings are shown in Fig. 2. The data stem from

Table 2: Mean values and standard deviations of some characteristics storm parameters. The P-values of the Wilcoxon test suggest that only the directions of the SR and SL storms are significantly different at the 5% level.

| Parameter | Mean/Standard deviation SL Storms | SR Storms | P-values of Wilcoxon test |
|---|---|---|---|
| Nr. of storms | 20 | 22 | |
| t > 59 dBZ (min) | 73/30 | 70/27 | 0.90 |
| Zm (dBZ) | 68.4/2.8 | 70.2/3.6 | 0.08 |
| Direction (Deg) | 232/22 | 264/21 | 0.00* |
| Velocity (m $s^{-1}$) | 10.1/4.1 | 11.5/4.3 | 0.39 |

the Payerne sounding, which is released daily at 12Z. Payerne is located 90 km to the west of the radar site. The pressure-weighted average wind vector was first computed for each individual sounding. The hodograph of a sounding was then turned in such a way that the mean-wind vector pointed toward the ENE. The vectors of the storm movement were rotated by the same angle as the individual hodographs. Taking the vector averages without such rotation would have led to a systematic underestimation of the wind speed, since the mean wind direction varies considerably from case to case.

The hodographs were grouped into three categories in Fig. 2: days with only SL storms, days with both SL and SR storms, and days with only SR storms. The mean hodographs for these three categories are generally similar. Each indicates a general tendency for the wind shear to veer with height, thus producing a generally clockwise-curved hodograph through a deep layer. The wind speed and shear seem to be somewhat larger in the "SR days only" category. Comparisons of these mean hodographs are, however, speculative since only about seven days worth of data

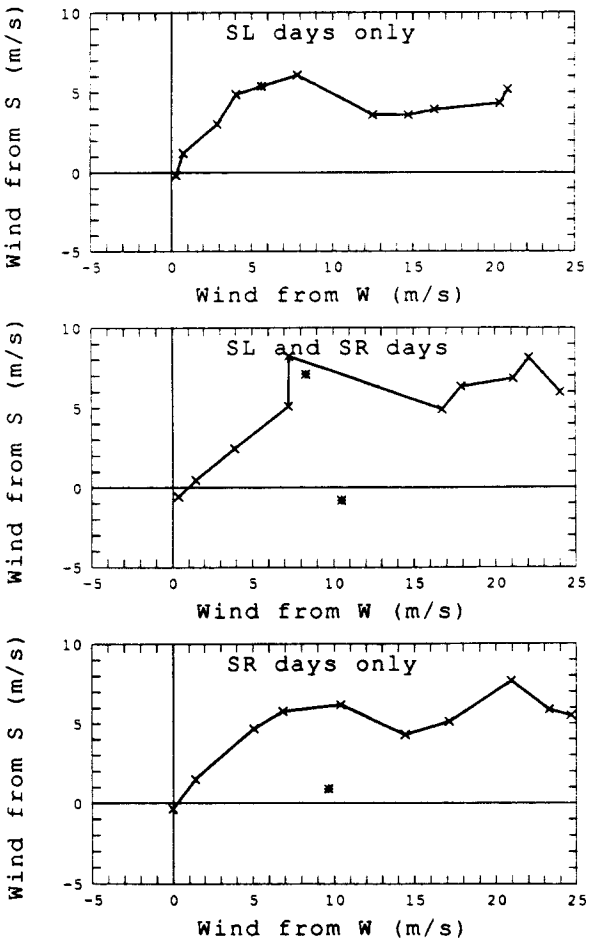


*Fig. 2: The mean hodographs for different storm categories. The crosses (x) mark the levels of 950, 900, 850, 800, 700, 500, 400, 300, 250, and 200 hPa (from left to right). The asterisks (*) mark the mean movement vector of the corresponding SL and SR storms.*

are used for each category (see Table 1).

The movement of the SL storms agrees well with the mean-environmental wind at the 700 hPa level. Although, at the same level, the SR storms move to the right of the mean-environmental wind. One could therefore question the suitability of the term "SL storm" in the present case. Perhaps the term "left-flank storm" (e.g. Weisman and Klemp 1984) may be more appropriate for the 700 hPa level. However, when taking the 500 hPa level instead of the 700 hPa level, one finds that the deviation of the storm movement from the mean-environmental wind is nearly the same magnitude for both storm classes, which means that the terms "SL" and "SR" storm can be used unambiguously with respect to the mean-environmental wind at 500 hPa.

The generally clockwise curvature of the hodographs for the three groupings in Fig. 2 is surprising since clockwise-curved hodographs are normally associated with right-moving supercell thunderstorms (Weisman and Klemp 1984; Klemp 1987). In the next section, we will see that although these mean hodographs from soundings were taken fairly far from where the storms occurred, they do not appear to indicate a predisposition toward left-moving storms. The low-level shear on an individual day in an area closer to where the storms actually occurred can turn counterclockwise while the shear at higher levels turns clockwise. This counterclockwise turning of the shear vector at low levels is apparently crucial in order to support the left-moving storms.

## 5. MODEL RESULTS

Some preliminary three-dimensional simulations have been made using a modified version of the Klemp-Wilhelmson (1978) cloud model. This version has optional ice-bulk microphysics based on the South Dakota parameterization (Lin et al. 1983) as implemented by Fovell and Ogura (1988), and conserves each class of moisture in the advection process. In addition, stretched grids are available in both horizontal directions. For these preliminary simulations, coarse resolution (2 km horizontal and 600 m vertical) and small, unstretched domains (100 km x 100 km x 20 km) have been employed.

At first, the model was initialized with the average temperature and moisture data representative of the "SL Days Only" class. This sounding has about 1160 J $kg^{-1}$ of CAPE with reference to a model surface parcel. We found that we could not get the convection to survive beyond the initial impulse unless some extra moisture was added to the sounding above 870 mb. We used the moisture sounding of one particular case, the 14 July 1978 event depicted in Fig. 1, as a guide for the moisture enhancement. The CAPE for the modified sounding, shown in Fig. 3, is the same as for the original since the surface temperature and moisture were unchanged.

An ice-free simulation using the "SL days only" hodograph was made and it produced a weak, nonsplitting storm which moved well to the right of the winds at any level. As expected, the activation of the ice-phase processes did little to alter the strength or propagation direction of the storm. This result appears to reinforce the notion that the mean Payerne soundings could not support left-moving storms. Evidently, these soundings did not contain subtle details of the environment in the specific region where the left-moving storms occurred. A sounding more representative of the conditions is needed in the immediate vicinity of the storm as a basis for a meaningful simulation.

Thus motivated, we made further simulations using the hodograph of the 14 July 1978 storm (displayed in Fig. 1) as this was a particularly well-observed splitting storm event and the only case for which special sounding data were available for a day on which left-moving storms occurred. According to Table 1, this storm belonged to the "SL and SR Days" class. Its hodograph, which is shown in Fig. 4a, has considerably more shear than the "SL Days Only", both over the entire troposphere and in midlevel

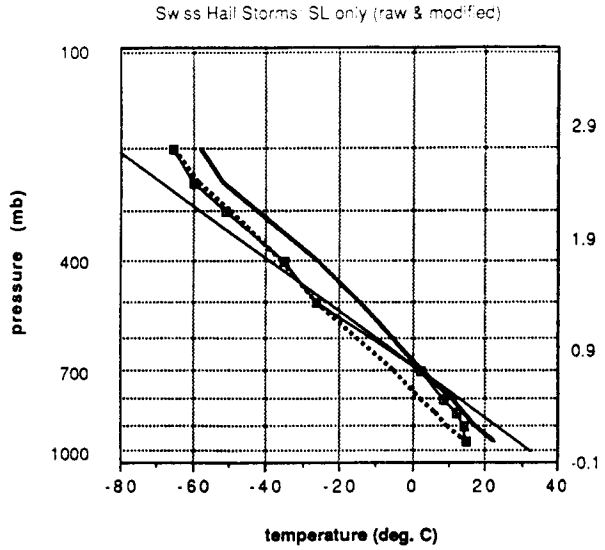


*Fig. 3 Average sounding for the "SL Days Only" class, showing dry-bulb temperature (thick solid line), original dew point temperature (thick broken line), and enhanced moisture profile (thin solid line).*

concentration. This is more apparent in the next two panels of Fig. 4, which present the profiles of the ground-relative easterly and northerly winds with height for both this case (Fig. 4b) and the "SL Days Only" class (Fig. 4c). The general shapes of the individual profiles between the two panels are the same, but the 14 July case clearly had more shear in both wind components. Most importantly, the $v$ component was northerly in the lowest 1.9 km. From 1.9 to 2.7 km, it reversed sharply back to southerly. This structure of the $v$ component of the wind in the lowest 2.7 km made the curvature of the hodograph in Fig. 4a counterclockwise in the lowest 2.7 km.

Simulations with and without the ice microphysics were made. Both simulations produced splitting storms. In the ice-free simulation, the left storm member moved from 243° at 10.4 m $s^{-1}$ and the right storm member moved from 290° at 11.3 m $s^{-1}$. These velocities are comparable to those of the observed storm members, which Table 1 shows moved from 248° at 8 m $s^{-1}$ for the left mover and from 290° at 13.0 m $s^{-1}$ for the right mover. In the ice case, the left mover was found to move somewhat faster, from 251° at 14.2 m $s^{-1}$; however, other than the differing propagation speed, the storm member appeared to be quite similar to that produced in the ice-free run. The limited domain size for these initial simulations prevented us from being able to keep both storms in the domain simultaneously for very long. The ice simulation was made to specifically track the left mover.

In both the ice and ice-free simulations, the right-moving member was at first the stronger of the two. It possessed a larger maximum updraft and produced more intense surface precipitation (Fig. 5). Rainfall intensities were smaller for both storm members in the ice simulation as the more complex microphysics slowed the conversion of condensate to rainwater. However, in the next half hour the left mover continued to strengthen while the right mover weakened, and at the end of this interval, the left mover became the stronger storm. By 10800 s, the right mover was virtually dead, even in the ice-free simulation which specifically tracked it; while the left mover survived beyond this time.

In the observed case, both a right mover and a left mover were able to exist for a long time on the same day, whereas the right-moving component of the model storm died. However, the observed right and left movers were not members of the same split. Instead they represent two cases, one in which the right mover survived and the other in which the left mover survived. The initial behavior of the model simulation, in which the right mover was actually stronger for a while, suggests that a very slight change in the local environment of the storm might easily have led to the survival of the right mover rather than the left mover. Apparently, the hodograph used in our simulation was more favorable to the left mover. It would be interesting to know what local differences in environment existed; however, only the one sounding was available.

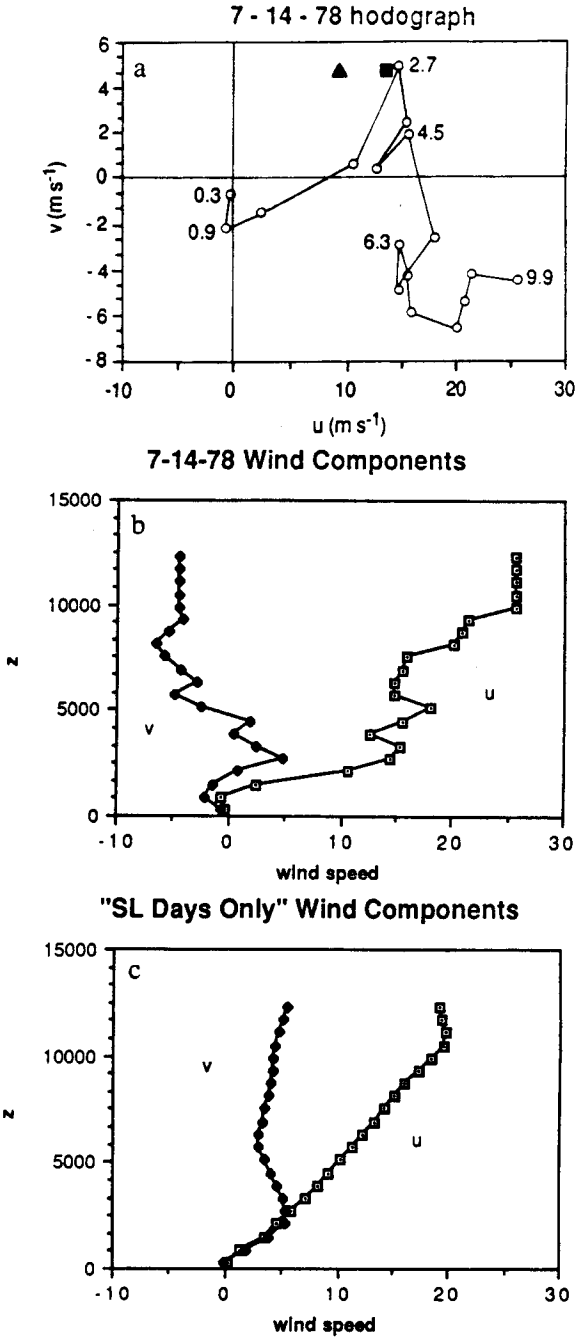


*Fig. 4 (a) Hodograph for the July 14, 1978 storm, taken at 14h (local time) at Gormund. Height in km is marked for some of the points. Storm speeds achieved by the model left mover for the ice-free and ice simulations are marked by the triangle and square, respectively. (b & c) Vertical wind profiles of easterly and northerly wind components for (b) the 14 July 1978 storm and (c) the average of the "SL Days Only" class.*

The echo structure developed by the model left-moving storm appears fairly realistic when compared to the actual left-moving storm (Fig. 1). Fig. 6 shows the model-estimated radar reflectivity field at 10800 sec for a portion of the domain surrounding the left mover. The plot is for 3.3 km above the model surface and was taken from the ice model simulation; we have zoomed in on a portion of the domain immediately surrounding the left-moving storm, which is moving to the NNE at 4.5 m $s^{-1}$ relative to the motion of this domain.

Clearly discernable in the figure is a distinct "hook" shape in the reflectivity field on the southeast (rear) side of the storm,

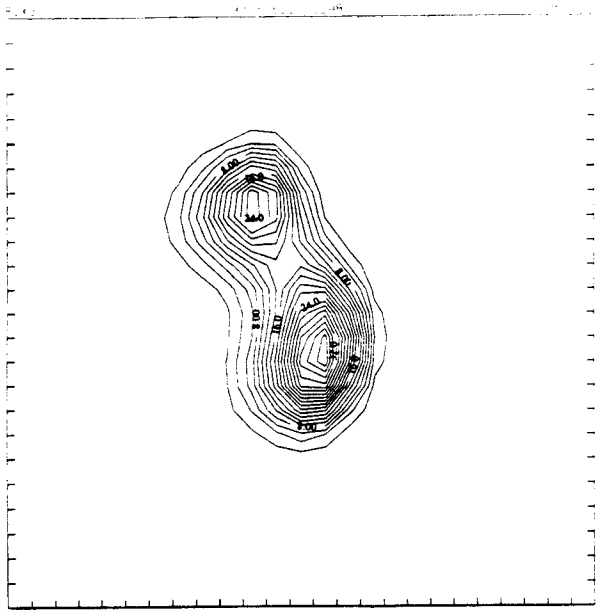

*Fig. 5 Estimated instantaneous rainfall-rate pattern from the ice model simulation of the July 14, 1987 case at 3600 sec. Only a 50 x 50 km portion of the computational domain is shown. Note that the storm has commenced splitting and the right mover is initially the stronger of the two.*

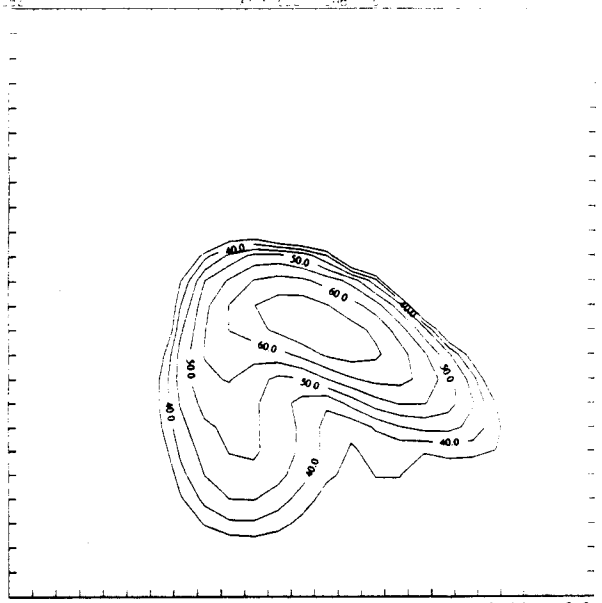

*Fig. 6 Model-estimated radar reflectivity (dBZ) field at 3.3 km above the model surface at 10800 sec for the July 14, 1978 simulation with ice processes activated. Only a 50 x 50 km portion of the domain immediately enclosing the left mover is shown.*

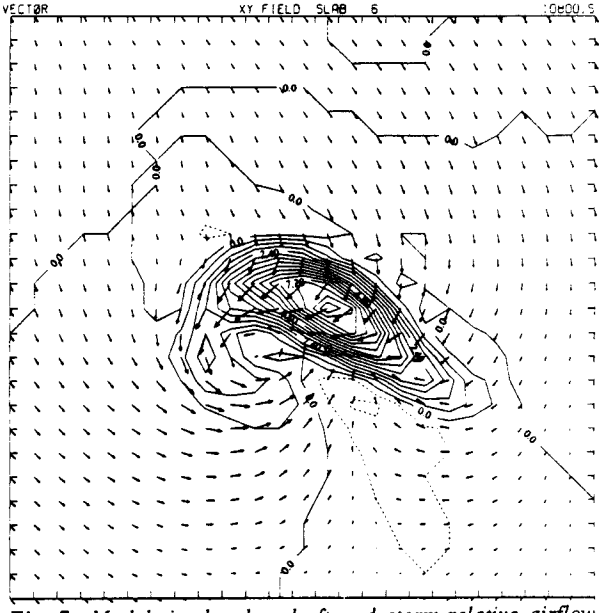


*Fig. 7 Model-simulated updraft and storm-relative airflow for the same level and time as Fig. 6. Although the airflow has been adjusted to be storm-relative, the storm is actually moving to the NNE at 4.5 m s$^{-1}$ in this subdomain.*

which is similar in location and orientation to that seen in the actual storm. As noted earlier, this is interesting since one would expect a true hook-echo feature to form on the north side of a left-moving storm. Analysis of the model data reveals that the "hook" feature of the model storm is, in fact, *not* a true hook in the sense of Lemon and Doswell (1979) since it is collocated with downdraft rather than with updraft. Like most (if not all) other left-moving storms, the updraft of the model storm was found to have anticyclonic rotation. This can be seen in Fig. 7 which depicts the storm-relative horizontal airflow overlapped with the vertical velocity at 3.3 km for the same subdomain as in Fig. 6. Comparison of the airflow in this figure with the echo in Fig. 6 suggests that the "hook" in this case was the result of advection of reflecting substances (rain and hail at this level) out of the updraft region. Examination of estimated reflectivity fields for the model storm across time suggests a cyclonic rotation of echo features observed in the actual storm, which is consistent with the airflow of the model storm.

So in this case, the left-moving storm of the model simulation is *not* a mirror image of a right mover for two basic reasons. First, the right-moving component of the model storm failed to survive, so the left-moving storm was clearly favored. Second, the left mover failed to develop a hook-echo feature on its northern flank, which is where it should have appeared if it was going to produce one. Instead, it produced what might be termed a "false hook" on its southern flank. The remarkable result is that this peculiar behavior corresponds exactly to what was observed on 14 July 1978, which is typical for the Swiss left-moving hailstorms.

We believe that this interesting behavior is a result of the complex hodograph structure. As noted previously, Fig. 4a is characterized below 2.7 km by counterclockwise curvature, with clockwise curvature above this level. Right-moving storms have been associated with clockwise-curved hodographs in previous modelling studies [see Klemp's (1987) review], and it is generally believed that left-moving storms are similarly associated with counterclockwise-curved hodographs. *It appears now, from our simulation, that only a shallow layer of counterclockwise curvature is sufficient to determine that the left-moving member of the split will be favored in the model simulation.* As discussed by Klemp (1987), the favoring of the left- (or right-) moving storm is a result of the rotational dynamics of the storm. The rotation produces a dynamically induced pressure-perturbation pattern in the storm, which favors the left-moving member when the environment hodograph has counterclockwise curvature. Further simulations need to be performed in order to gauge the effect of the clockwise shear above low levels on the structure and behavior of the storm and to determine why only the shallow layer of counterclockwise curvature is necessary to favor the left-moving storm.

We further note that our results, which simulate the behavior of the observed left-moving storm, were achieved in a model domain with a perfectly flat lower boundary. Hence, there is no need to suppose that the local topography directly causes the left mover to be favored in this case.

It is evident from Fig. 4b that the counterclockwise curvature of the low-level hodograph was associated with the weak northerly flow in the lowest levels. This situation is different from that found in the central U.S., where a strong southerly low-level flow of moist air is often observed in connection with the outbreak of tornadic thunderstorms (e.g. Maddox 1976). In central Switzerland, the Alps act as a barrier

against the advection of moist air from the Mediterranean Sea to the south. In addition, there may be an effect of the specific orographic pattern at the northwestern flank of the Swiss Alps. A local circulation of moist low-level air may develop on sunny days from the NW towards the hilly regions where thunderstorms form. This circulation may account for the deformation of the hodograph into a counterclockwise-curved shape at low levels. Thus, while the topography does not affect the dynamics of the model storm directly through a non-flat lower boundary, it may have an indirect effect on storm dynamics by modifying the environmental wind profile in the vicinity of the storm. Continuous wind measurements of a dense network of alpine ground stations are available for at least a part of the documented thunderstorm days. These data will be analyzed in detail in order to see if the discussed local wind effect is a characteristic feature of the days when SL storms occur.

## 6. CONCLUSIONS

Carefully calibrated 10-cm radar data were collected in central Switzerland during an eight-year period. The 42 most severe hailstorms have been selected from these data and examined with respect to their movement and structure in relation to the environmental wind. It was found that the severe left-moving hailstorms are nearly as frequent as their right-moving counterparts: 20 storms were left-moving, while 22 were right-moving.

The average values of intensity, duration, and velocity are very similar for both storm classes. The values of maximum reflectivity are somewhat higher for the SR storms than for the SL storms when the storm velocity is larger than 15 m $s^{-1}$. The SL storms are not a mirror image of the right-moving storms that occur in the U.S. The SL storms often show a "false" hook-echo structure. The hook echo is found on the right-rear flank with respect to the movement of the storms and exhibits cyclonic rotation. Mean-wind hodographs constructed from synoptic-sounding data taken far from the storm region indicated only clockwise turning of the mean-environmental wind shear in the lowest 5 km for all storm classes. However, a sounding taken closer to the region where an SL storm occurred (on 14 July 1978) exhibited a shallow layer of counterclockwise curvature below 2.7-km altitude. Above this height the curvature changed to clockwise. The counterclockwise curvature at low levels was associated with a northerly component of the wind in the lowest 1.9 km. This northerly component may have been induced by heating over the Alps to the south of the storm area.

A three-dimensional numerical model simulation demonstrates that the shear in the environment on 14 July 1978 was sufficiently strong enough to support storm splitting. Initially, there was a short period in which the right-moving member of the split was stronger; however, eventually the left-moving member survived while the right mover died. Evidently, the shallow layer of counterclockwise curvature in the hodograph was sufficient to allow the internal rotational dynamics to favor the left-moving member. The model simulation reproduced the cyclonically rotating "false" hook, which was found to be centered in the downdraft zone. The updraft was located on the northern flank and exhibited anticyclonic rotation. This similarity to the observations lends confidence to the model results.

Since the SL storms are responsible for a non-negligible part of the total hail damage in central Switzerland, a better knowledge of these storms will facilitate the future assessment of protection systems against hail. The observational and modelling work reported here will therefore be extended. The observational base will be improved by making Doppler-radar measurements to document the internal rotational structure of the storms and by obtaining sounding data of the vertical wind profile more closely associated with the storms. With these new data, more detailed comparisons between the model simulations and the data will be possible. Future work with the numerical model can then be directed toward an understanding of the hail formation mechanisms in the Swiss type of hailstorm and toward a better understanding of the dynamics giving rise to both the left- and right-moving storms.

## ACKNOWLEDGMENTS

J. Bader helped to prepare and analyze the data, Professor A. Waldvogel reviewed the manuscript, and G.C. Gudmundson edited the manuscript. These contributions are gratefully acknowledged. The participation of R. Houze and R. Fovell in this study was supported in part by the U.S. National Science Foundation under grant ATM-8719838. The Swiss Federal College of Technology (ETH) and the University of Washington made it possible for Professor Houze to spend a year in residence at ETH. The model simulations were made at NCSA.

## REFERENCES

Achtemeier, G.L., 1975: Doppler velocity and reflectivity morphology of a severe left-moving split thunderstorm. Preprints, *16th Conf. Radar Meteorology*, Houston, Amer. Meteor. Soc., 93-98.

Aydin, K., T.A. Seliga and V. Balaji, 1986: Remote sensing of hail with a dual-linear polarization radar. *J. Climate Appl. Meteor.*, **25**, 1475-1484.

Browning, K.A., 1968: The organization of severe local storms. *Weather*, **23**, 429-434.

Chisholm, A.J., and J.H. Renick, 1972: The kinematics of multicell and supercell Alberta hailstorms. Research Council of Alberta Hail Studies Rep. No. 72-2, 24-31.

Federer, B., A. Waldvogel, W. Schmid, H.-H. Schiesser, F. Hampel, M. Schweingruber, W. Stahel, J. Bader, J.F. Mezeix, N. Doras, G. d'Aubigny, G. DerMegreditchian and D. Vento, 1986: Main results of Grossversuch IV. *J. Climate Appl. Meteor.*, **25**, 917-957.

Fovell, R., and Y. Ogura, 1988: Numerical simulation of a midlatitude squall line in two dimensions. *J. Atmos. Sci.*, **45**, 3846-3879.

Klemp, J.B., 1987: Dynamics of tornadic thunderstorms. *Ann. Rev. Fluid. Mech.*, **19**, 369-402.

Klemp, J.B., and R.B.Wilhelmson, 1978: The simulation of three-dimensional convective storm dynamics. *J. Atmos. Sci.*, **35**, 1070-1096.

Lemon, L.R., and C.A. Doswell, 1979: Mesocyclone and severe thunderstorm structure: a revised model. Preprints, *11th Conf. Severe Local Storms*, Kansas City, Amer. Meteor. Soc., 458-463.

Lin, Y.-L., R.D. Farley and H.D. Orville, 1983: Bulk parameterization of the snow field in a cloud model. *J. Climate Appl. Meteor.*, **22**, 1065-1092.

Maddox, R.A., 1976: An evaluation of tornado proximity wind and stability data. *Mon. Wea. Rev.*, **104**, 133-142.

Schiesser, H.-H., 1990: Hailfall: The relationship between radar measurements and crop damage. Accepted for publication in *Atmos. Research*.

Tripoli, G.J., and W.R. Cotton, 1986: An intense, quasi-steady thunderstorm over mountainous terrain. Part IV: Three-dimensional numerical simulation. *J. Atmos. Sci.*, **43**, 894-912.

Waldvogel, A., B. Federer, W. Schmid and J.F. Mezeix, 1978: The kinetic energy of hailfalls. Part II: Radar and hailpads. *J. Appl. Meteor.*, **17**, 1680-1693.

Waldvogel, A., and W. Schmid, 1982: The kinetic energy of hailfalls. Part III: Sampling errors inferred from radar data. *J. Appl. Meteor.*, **21**, 1228-1238.

Waldvogel, A., and W. Schmid, 1983: Single wavelength radar measurements of hailfall kinetic energy. Preprints, *21st Conf. Radar Meteorology*, Edmonton, Amer. Meteor. Soc., 425-428.

Weisman, M.L., and J.B. Klemp, 1984: The structure and classification of numerically simulated convective storms in directionally varying wind shears. *Mon. Wea. Rev.*, **112**, 2479-2498.